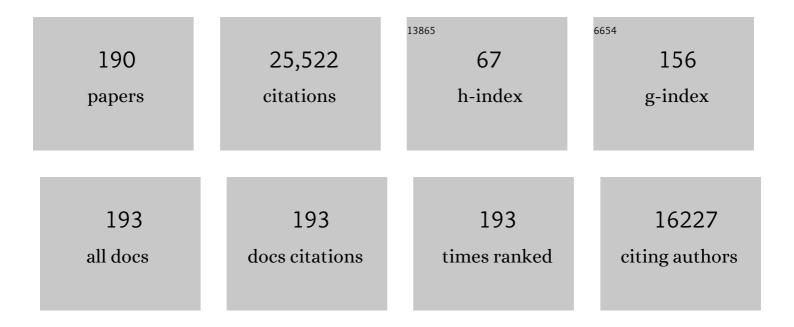
## List of Publications by Year in descending order

Source: https://exaly.com/author-pdf/3288632/publications.pdf Version: 2024-02-01



FENC CAO

#	Article	IF	CITATIONS
1	Global land cover mapping from MODIS: algorithms and early results. Remote Sensing of Environment, 2002, 83, 287-302.	11.0	2,256
2	First operational BRDF, albedo nadir reflectance products from MODIS. Remote Sensing of Environment, 2002, 83, 135-148.	11.0	2,022
3	Monitoring vegetation phenology using MODIS. Remote Sensing of Environment, 2003, 84, 471-475.	11.0	1,948
4	Landsat-8: Science and product vision for terrestrial global change research. Remote Sensing of Environment, 2014, 145, 154-172.	11.0	1,599
5	On the blending of the Landsat and MODIS surface reflectance: predicting daily Landsat surface reflectance. IEEE Transactions on Geoscience and Remote Sensing, 2006, 44, 2207-2218.	6.3	1,321
6	A Landsat Surface Reflectance Dataset for North America, 1990–2000. IEEE Geoscience and Remote Sensing Letters, 2006, 3, 68-72.	3.1	1,279
7	An enhanced spatial and temporal adaptive reflectance fusion model for complex heterogeneous regions. Remote Sensing of Environment, 2010, 114, 2610-2623.	11.0	929
8	Free Access to Landsat Imagery. Science, 2008, 320, 1011-1011.	12.6	727
9	Current status of Landsat program, science, and applications. Remote Sensing of Environment, 2019, 225, 127-147.	11.0	586
10	A new data fusion model for high spatial- and temporal-resolution mapping of forest disturbance based on Landsat and MODIS. Remote Sensing of Environment, 2009, 113, 1613-1627.	11.0	567
11	A flexible spatiotemporal method for fusing satellite images with different resolutions. Remote Sensing of Environment, 2016, 172, 165-177.	11.0	461
12	Mapping daily evapotranspiration at field to continental scales using geostationary and polar orbiting satellite imagery. Hydrology and Earth System Sciences, 2011, 15, 223-239.	4.9	454
13	Multi-temporal MODIS–Landsat data fusion for relative radiometric normalization, gap filling, and prediction of Landsat data. Remote Sensing of Environment, 2008, 112, 3112-3130.	11.0	430
14	Generating daily land surface temperature at Landsat resolution by fusing Landsat and MODIS data. Remote Sensing of Environment, 2014, 145, 55-67.	11.0	399
15	A simple and effective method for filling gaps in Landsat ETM+ SLC-off images. Remote Sensing of Environment, 2011, 115, 1053-1064.	11.0	395
16	Toward mapping crop progress at field scales through fusion of Landsat and MODIS imagery. Remote Sensing of Environment, 2017, 188, 9-25.	11.0	340
17	Global characterization and monitoring of forest cover using Landsat data: opportunities and challenges. International Journal of Digital Earth, 2012, 5, 373-397.	3.9	252
18	Inversion methods for physicallyâ€based models. International Journal of Remote Sensing, 2000, 18, 381-439.	1.0	248

#	Article	IF	CITATIONS
19	Spatially complete global spectral surface albedos: value-added datasets derived from Terra MODIS land products. IEEE Transactions on Geoscience and Remote Sensing, 2005, 43, 144-158.	6.3	244
20	Generation of dense time series synthetic Landsat data through data blending with MODIS using a spatial and temporal adaptive reflectance fusion model. Remote Sensing of Environment, 2009, 113, 1988-1999.	11.0	244
21	Evaluation of Landsat and MODIS data fusion products for analysis of dryland forest phenology. Remote Sensing of Environment, 2012, 117, 381-393.	11.0	240
22	The Evaporative Stress Index as an indicator of agricultural drought in Brazil: An assessment based on crop yield impacts. Remote Sensing of Environment, 2016, 174, 82-99.	11.0	238
23	Accuracy assessment of the MODIS 16-day albedo product for snow: comparisons with Greenland in situ measurements. Remote Sensing of Environment, 2005, 94, 46-60.	11.0	228
24	Fusing Landsat and MODIS Data for Vegetation Monitoring. IEEE Geoscience and Remote Sensing Magazine, 2015, 3, 47-60.	9.6	216
25	Assessing the coupling between surface albedo derived from MODIS and the fraction of diffuse skylight over spatially-characterized landscapes. Remote Sensing of Environment, 2010, 114, 738-760.	11.0	204
26	Monitoring daily evapotranspiration over two California vineyards using Landsat 8 in a multi-sensor data fusion approach. Remote Sensing of Environment, 2016, 185, 155-170.	11.0	200
27	An algorithm for the retrieval of 30-m snow-free albedo from Landsat surface reflectance and MODIS BRDF. Remote Sensing of Environment, 2011, 115, 2204-2216.	11.0	192
28	An Algorithm to Produce Temporally and Spatially Continuous MODIS-LAI Time Series. IEEE Geoscience and Remote Sensing Letters, 2008, 5, 60-64.	3.1	189
29	An Enhanced TIMESAT Algorithm for Estimating Vegetation Phenology Metrics From MODIS Data. IEEE Journal of Selected Topics in Applied Earth Observations and Remote Sensing, 2011, 4, 361-371.	4.9	181
30	Mapping daily evapotranspiration at field scales over rainfed and irrigated agricultural areas using remote sensing data fusion. Agricultural and Forest Meteorology, 2014, 186, 1-11.	4.8	178
31	Consistency of MODIS surface bidirectional reflectance distribution function and albedo retrievals: 2. Validation. Journal of Geophysical Research, 2003, 108, .	3.3	177
32	Representative lake water extent mapping at continental scales using multi-temporal Landsat-8 imagery. Remote Sensing of Environment, 2016, 185, 129-141.	11.0	175
33	A Data Mining Approach for Sharpening Thermal Satellite Imagery over Land. Remote Sensing, 2012, 4, 3287-3319.	4.0	171
34	Validation of the MODIS bidirectional reflectance distribution function and albedo retrievals using combined observations from the aqua and terra platforms. IEEE Transactions on Geoscience and Remote Sensing, 2006, 44, 1555-1565.	6.3	169
35	Exploration of scaling effects on coarse resolution land surface phenology. Remote Sensing of Environment, 2017, 190, 318-330.	11.0	149
36	A data fusion approach for mapping daily evapotranspiration at field scale. Water Resources Research, 2013, 49, 4672-4686.	4.2	142

#	Article	IF	CITATIONS
37	MODIS bidirectional reflectance distribution function and albedo Climate Modeling Grid products and the variability of albedo for major global vegetation types. Journal of Geophysical Research, 2005, 110, .	3.3	140
38	A Modified Neighborhood Similar Pixel Interpolator Approach for Removing Thick Clouds in Landsat Images. IEEE Geoscience and Remote Sensing Letters, 2012, 9, 521-525.	3.1	128
39	A priori knowledge accumulation and its application to linear BRDF model inversion. Journal of Geophysical Research, 2001, 106, 11925-11935.	3.3	126
40	Daily Mapping of 30 m LAI and NDVI for Grape Yield Prediction in California Vineyards. Remote Sensing, 2017, 9, 317.	4.0	126
41	Consistency of MODIS surface bidirectional reflectance distribution function and albedo retrievals: 1. Algorithm performance. Journal of Geophysical Research, 2003, 108, .	3.3	121
42	Comparison of seasonal and spatial variations of albedos from Moderate-Resolution Imaging Spectroradiometer (MODIS) and Common Land Model. Journal of Geophysical Research, 2003, 108, .	3.3	120
43	Detecting vegetation structure using a kernel-based BRDF model. Remote Sensing of Environment, 2003, 86, 198-205.	11.0	117
44	Generating global Leaf Area Index from Landsat: Algorithm formulation and demonstration. Remote Sensing of Environment, 2012, 122, 185-202.	11.0	115
45	Joint leaf chlorophyll content and leaf area index retrieval from Landsat data using a regularized model inversion system (REGFLEC). Remote Sensing of Environment, 2015, 159, 203-221.	11.0	114
46	Development of time series stacks of Landsat images for reconstructing forest disturbance history. International Journal of Digital Earth, 2009, 2, 195-218.	3.9	112
47	Mapping daily evapotranspiration at Landsat spatial scales during the BEAREX'08 field campaign. Advances in Water Resources, 2012, 50, 162-177.	3.8	111
48	Evapotranspiration estimates derived using thermal-based satellite remote sensing and data fusion for irrigation management in California vineyards. Irrigation Science, 2019, 37, 431-449.	2.8	95
49	Assessment of global climate model land surface albedo using MODIS data. Geophysical Research Letters, 2003, 30, .	4.0	92
50	Global surface reflectance products from Landsat: Assessment using coincident MODIS observations. Remote Sensing of Environment, 2013, 134, 276-293.	11.0	92
51	Evaluating land surface albedo estimation from Landsat MSS, TM, ETM +, and OLI data based on the unified direct estimation approach. Remote Sensing of Environment, 2018, 204, 181-196.	11.0	91
52	Using MODIS BRDF and Albedo Data to Evaluate Global Model Land Surface Albedo. Journal of Hydrometeorology, 2004, 5, 3-14.	1.9	90
53	Use of In Situ and Airborne Multiangle Data to Assess MODIS- and Landsat-Based Estimates of Directional Reflectance and Albedo. IEEE Transactions on Geoscience and Remote Sensing, 2013, 51, 1393-1404.	6.3	90
54	Mapping impervious surface expansion using medium-resolution satellite image time series: a case study in the Yangtze River Delta, China. International Journal of Remote Sensing, 2012, 33, 7609-7628.	2.9	88

#	Article	IF	CITATIONS
55	The Grape Remote Sensing Atmospheric Profile and Evapotranspiration Experiment. Bulletin of the American Meteorological Society, 2018, 99, 1791-1812.	3.3	88
56	Evaluation of TSEB turbulent fluxes using different methods for the retrieval of soil and canopy component temperatures from UAV thermal and multispectral imagery. Irrigation Science, 2019, 37, 389-406.	2.8	84
57	Improved forest change detection with terrain illumination corrected Landsat images. Remote Sensing of Environment, 2013, 136, 469-483.	11.0	83
58	Reconstructing daily clear-sky land surface temperature for cloudy regions from MODIS data. Computers and Geosciences, 2017, 105, 10-20.	4.2	83
59	Development of land surface albedo parameterization based on Moderate Resolution Imaging Spectroradiometer (MODIS) data. Journal of Geophysical Research, 2005, 110, .	3.3	81
60	How does snow impact the albedo of vegetated land surfaces as analyzed with MODIS data?. Geophysical Research Letters, 2002, 29, 12-1-12-4.	4.0	80
61	Field-Scale Assessment of Land and Water Use Change over the California Delta Using Remote Sensing. Remote Sensing, 2018, 10, 889.	4.0	79
62	Mapping evapotranspiration with high-resolution aircraft imagery over vineyards using one- and two-source modeling schemes. Hydrology and Earth System Sciences, 2016, 20, 1523-1545.	4.9	78
63	Daily Landsat-scale evapotranspiration estimation over a forested landscape in North Carolina, USA, using multi-satellite data fusion. Hydrology and Earth System Sciences, 2017, 21, 1017-1037.	4.9	77
64	Mapping Crop Phenology in Near Real-Time Using Satellite Remote Sensing: Challenges and Opportunities. Journal of Remote Sensing, 2021, 2021, .	6.7	77
65	Field-scale mapping of evaporative stress indicators of crop yield: An application over Mead, NE, USA. Remote Sensing of Environment, 2018, 210, 387-402.	11.0	75
66	Assessing the Variability of Corn and Soybean Yields in Central Iowa Using High Spatiotemporal Resolution Multi-Satellite Imagery. Remote Sensing, 2018, 10, 1489.	4.0	72
67	A within-season approach for detecting early growth stages in corn and soybean using high temporal and spatial resolution imagery. Remote Sensing of Environment, 2020, 242, 111752.	11.0	71
68	Interoperability of ECOSTRESS and Landsat for mapping evapotranspiration time series at sub-field scales. Remote Sensing of Environment, 2021, 252, 112189.	11.0	71
69	Development and evaluation of a new algorithm for detecting 30Âm land surface phenology from VIIRS and HLS time series. ISPRS Journal of Photogrammetry and Remote Sensing, 2020, 161, 37-51.	11.1	69
70	Bidirectional NDVI and atmospherically resistant BRDF inversion for vegetation canopy. IEEE Transactions on Geoscience and Remote Sensing, 2002, 40, 1269-1278.	6.3	68
71	Relating MODIS-derived surface albedo to soils and rock types over Northern Africa and the Arabian peninsula. Geophysical Research Letters, 2002, 29, 67-1-67-4.	4.0	67
72	An approach for the long-term 30-m land surface snow-free albedo retrieval from historic Landsat surface reflectance and MODIS-based a priori anisotropy knowledge. Remote Sensing of Environment, 2014, 152, 467-479.	11.0	64

#	Article	IF	CITATIONS
73	Improving MODIS surface BRDF/Albedo retrieval with MISR multiangle observations. IEEE Transactions on Geoscience and Remote Sensing, 2002, 40, 1593-1604.	6.3	62
74	Operational Data Fusion Framework for Building Frequent Landsat-Like Imagery. IEEE Transactions on Geoscience and Remote Sensing, 2014, 52, 7353-7365.	6.3	62
75	Aqua and Terra MODIS Albedo and Reflectance Anisotropy Products. Remote Sensing and Digital Image Processing, 2010, , 549-561.	0.7	62
76	Comparison of satellite-derived LAI and precipitation anomalies over Brazil with a thermal infrared-based Evaporative Stress Index for 2003–2013. Journal of Hydrology, 2015, 526, 287-302.	5.4	61
77	Greenland surface albedo changes in July 1981–2012 from satellite observations. Environmental Research Letters, 2013, 8, 044043.	5.2	59
78	Estimation of crop gross primary production (GPP): fAPARchl versus MOD15A2 FPAR. Remote Sensing of Environment, 2014, 153, 1-6.	11.0	58
79	Angular Effects and Correction for Medium Resolution Sensors to Support Crop Monitoring. IEEE Journal of Selected Topics in Applied Earth Observations and Remote Sensing, 2014, 7, 4480-4489.	4.9	57
80	Land boundary conditions from MODIS data and consequences for the albedo of a climate model. Geophysical Research Letters, 2004, 31, n/a-n/a.	4.0	52
81	A Hybrid Color Mapping Approach to Fusing MODIS and Landsat Images for Forward Prediction. Remote Sensing, 2018, 10, 520.	4.0	51
82	Utility of the two-source energy balance (TSEB) model in vine and interrow flux partitioning over the growing season. Irrigation Science, 2019, 37, 375-388.	2.8	50
83	Monitoring land surface albedo and vegetation dynamics using high spatial and temporal resolution synthetic time series from Landsat and the MODIS BRDF/NBAR/albedo product. International Journal of Applied Earth Observation and Geoinformation, 2017, 59, 104-117.	2.8	49
84	A Spatio-Temporal Enhancement Method for medium resolution LAI (STEM-LAI). International Journal of Applied Earth Observation and Geoinformation, 2016, 47, 15-29.	2.8	48
85	Investigating water use over the <scp>C</scp> hoptank <scp>R</scp> iver <scp>W</scp> atershed using a multisatellite data fusion approach. Water Resources Research, 2017, 53, 5298-5319.	4.2	48
86	Characterization of North American land cover from NOAA-AVHRR data using the EOS MODIS Land Cover Classification Algorithm. Geophysical Research Letters, 2000, 27, 977-980.	4.0	47
87	Use of Moderate-Resolution Imaging Spectroradiometer bidirectional reflectance distribution function products to enhance simulated surface albedos. Journal of Geophysical Research, 2004, 109, .	3.3	47
88	Data assimilation of high-resolution thermal and radar remote sensing retrievals for soil moisture monitoring in a drip-irrigated vineyard. Remote Sensing of Environment, 2020, 239, 111622.	11.0	46
89	Global albedo change and radiative cooling from anthropogenic land cover change, 1700 to 2005 based on MODIS, land use harmonization, radiative kernels, and reanalysis. Geophysical Research Letters, 2014, 41, 9087-9096.	4.0	44

#	Article	IF	CITATIONS
91	Investigating impacts of drought and disturbance on evapotranspiration over a forested landscape in North Carolina, USA using high spatiotemporal resolution remotely sensed data. Remote Sensing of Environment, 2020, 238, 111018.	11.0	41
92	Relationships between the evaporative stress index and winter wheat and spring barley yield anomalies in the Czech Republic. Climate Research, 2016, 70, 215-230.	1.1	41
93	Impact of Tile Drainage on Evapotranspiration in South Dakota, USA, Based on High Spatiotemporal Resolution Evapotranspiration Time Series From a Multisatellite Data Fusion System. IEEE Journal of Selected Topics in Applied Earth Observations and Remote Sensing, 2017, 10, 2550-2564.	4.9	40
94	Assessment of Leaf Area Index Models Using Harmonized Landsat and Sentinel-2 Surface Reflectance Data over a Semi-Arid Irrigated Landscape. Remote Sensing, 2020, 12, 3121.	4.0	39
95	Improving Spatial-Temporal Data Fusion by Choosing Optimal Input Image Pairs. Remote Sensing, 2018, 10, 1142.	4.0	38
96	Using a multikernel least-variance approach to retrieve and evaluate albedo from limited bidirectional measurements. Remote Sensing of Environment, 2001, 76, 57-66.	11.0	37
97	Coupling of phenological information and simulated vegetation index time series: Limitations and potentials for the assessment and monitoring of soil erosion risk. Catena, 2017, 150, 192-205.	5.0	36
98	A Cross Comparison of Spatiotemporally Enhanced Springtime Phenological Measurements From Satellites and Ground in a Northern U.S. Mixed Forest. IEEE Transactions on Geoscience and Remote Sensing, 2014, 52, 7513-7526.	6.3	35
99	Assessment of Spatiotemporal Fusion Algorithms for Planet and Worldview Images. Sensors, 2018, 18, 1051.	3.8	35
100	Using High-Spatiotemporal Thermal Satellite ET Retrievals for Operational Water Use and Stress Monitoring in a California Vineyard. Remote Sensing, 2019, 11, 2124.	4.0	35
101	Reconstructing daily 30Âm NDVI over complex agricultural landscapes using a crop reference curve approach. Remote Sensing of Environment, 2021, 253, 112156.	11.0	35
102	Studying drought-induced forest mortality using high spatiotemporal resolution evapotranspiration data from thermal satellite imaging. Remote Sensing of Environment, 2021, 265, 112640.	11.0	34
103	Evaluation of the Li transit kernel for BRDF modeling. International Journal of Remote Sensing, 2000, 19, 205-224.	1.0	33
104	Evaluation of ASTER-Like Daily Land Surface Temperature by Fusing ASTER and MODIS Data during the HiWATER-MUSOEXE. Remote Sensing, 2016, 8, 75.	4.0	33
105	Assessing the performance of a physically-based soil moisture module integrated within the Soil and Water Assessment Tool. Environmental Modelling and Software, 2018, 109, 329-341.	4.5	33
106	A data-driven approach to estimate leaf area index for Landsat images over the contiguous US. Remote Sensing of Environment, 2021, 258, 112383.	11.0	33
107	Real-Time Monitoring of Crop Phenology in the Midwestern United States Using VIIRS Observations. Remote Sensing, 2018, 10, 1540.	4.0	32
108	Multiscale climatological albedo look-up maps derived from moderate resolution imaging spectroradiometer BRDF/albedo products. Journal of Applied Remote Sensing, 2014, 8, 083532.	1.3	31

#	Article	IF	CITATIONS
109	Sharpening ECOSTRESS and VIIRS land surface temperature using harmonized Landsat-Sentinel surface reflectances. Remote Sensing of Environment, 2020, 251, 112055.	11.0	30
110	Using high-spatiotemporal thermal satellite ET retrievals to monitor water use over California vineyards of different climate, vine variety and trellis design. Agricultural Water Management, 2020, 241, 106361.	5.6	30
111	Retrieving Leaf Area Index From Landsat Using MODIS LAI Products and Field Measurements. IEEE Geoscience and Remote Sensing Letters, 2014, 11, 773-777.	3.1	29
112	Mapping Paddy Rice Area and Yields Over Thai Binh Province in Viet Nam From MODIS, Landsat, and ALOS-2/PALSAR-2. IEEE Journal of Selected Topics in Applied Earth Observations and Remote Sensing, 2018, 11, 2238-2252.	4.9	28
113	Influence of wind direction on the surface roughness of vineyards. Irrigation Science, 2019, 37, 359-373.	2.8	26
114	Relationships between soil water content, evapotranspiration, and irrigation measurements in a California drip-irrigated Pinot noir vineyard. Agricultural Water Management, 2020, 237, 106186.	5.6	26
115	Determining a robust indirect measurement of leaf area index in California vineyards for validating remote sensing-based retrievals. Irrigation Science, 2019, 37, 269-280.	2.8	25
116	Global climate forcing from albedo change caused by large-scale deforestation and reforestation: quantification and attribution of geographic variation. Climatic Change, 2017, 142, 463-476.	3.6	23
117	Impact of different within-canopy wind attenuation formulations on modelling sensible heat flux using TSEB. Irrigation Science, 2019, 37, 315-331.	2.8	23
118	Improving MODIS land cover classification by combining MODIS spectral and angular signatures in a Canadian boreal forest. Canadian Journal of Remote Sensing, 2011, 37, 184-203.	2.4	22
119	Impact of Insolation Data Source on Remote Sensing Retrievals of Evapotranspiration over the California Delta. Remote Sensing, 2019, 11, 216.	4.0	22
120	A multi-year intercomparison of micrometeorological observations at adjacent vineyards in California's Central Valley during GRAPEX. Irrigation Science, 2019, 37, 345-357.	2.8	22
121	Detecting Cover Crop End-Of-Season Using VENµS and Sentinel-2 Satellite Imagery. Remote Sensing, 2020, 12, 3524.	4.0	22
122	Spatial and temporal variability in Moderate Resolution Imaging Spectroradiometer–derived surface albedo over global arid regions. Journal of Geophysical Research, 2006, 111, .	3.3	21
123	Using APAR to Predict Aboveground Plant Productivity in Semi-Aid Rangelands: Spatial and Temporal Relationships Differ. Remote Sensing, 2018, 10, 1474.	4.0	21
124	Mapping Daily Evapotranspiration at Field Scale Using the Harmonized Landsat and Sentinel-2 Dataset, with Sharpened VIIRS as a Sentinel-2 Thermal Proxy. Remote Sensing, 2021, 13, 3420.	4.0	20
125	Temporally smoothed and gapâ€filled MODIS land products for carbon modelling: application of the fPAR product. International Journal of Remote Sensing, 2009, 30, 1083-1090.	2.9	19
126	Evaluation of the suitability of Landsat, MERIS, and MODIS for identifying spatial distribution patterns of total suspended matter from a self-organizing map (SOM) perspective. Catena, 2019, 172, 699-710.	5.0	18

# ARTICLE IF CITATIONS Phenological corrections to a field-scale, ET-based crop stress indicator: An application to yield 11.0 forecasting across the U.S. Corn Belt. Remote Sensing of Environment, 2021, 257, 112337. Derivation and validation of a new kernel for kernel-driven BRDF models., 1999, , . 128 16 129 Vegetation Phenology Metrics Derived from Temporally Smoothed and Gap-Filled MODIS Data., 2008, , . Micro-scale spatial variability in soil heat flux (SHF) in a wine-grape vineyard. Irrigation Science, 2019, 130 2.8 15 37, 253-268. Re-understanding of land surface albedo and related terms in satellite-based retrievals. Big Earth Data, 2020, 4, 45-67. 4.4 14 Hybrid phenology matching model for robust crop phenological retrieval. ISPRS Journal of Photogrammetry and Remote Sensing, 2021, 181, 308-326. 132 11.1 14 LAI estimation across California vineyards using sUAS multi-seasonal multi-spectral, thermal, and 2.8 14 elevation information and machine learning. Irrigation Science, 2022, 40, 731-759. Crop Growth Condition Assessment at County Scale Based on Heat-Aligned Growth Stages. Remote 134 4.0 13 Sensing, 2019, 11, 2439. Determining Evapotranspiration by Using Combination Equation Models with Sentinel-2 Data and Comparison with Thermal-Based Energy Balance in a California Irrigated Vineyard. Remote Sensing, 4.0 2021, 13, 3720. Improved Daily Evapotranspiration Estimation Using Remotely Sensed Data in a Data Fusion System. 136 4.0 13 Remote Sensing, 2022, 14, 1772. Evaluation of satellite Leaf Area Index in California vineyards for improving water use estimation. 2.8 Irrigation Science, 2022, 40, 531-551. Adaptive Selective Learning for automatic identification of sub-kilometer craters. Neurocomputing, 138 5.9 12 2012, 92, 78-87. Mapping daily leaf area index at 30 m resolution over a meadow steppe area by fusing Landsat, Sentinel-2A and MODIS data. International Journal of Remote Sensing, 2018, 39, 9025-9053. Mapping Climatological Bare Soil Albedos over the Contiguous United States Using MODIS Data. 140 4.0 12 Remote Sensing, 2019, 11, 666. Using Satellite Thermal-Based Evapotranspiration Time Series for Defining Management Zones and 141 Spatial Association to Local Attributes in a Vineyard. Remote Sensing, 2020, 12, 2436. Impact of advection on two-source energy balance (TSEB) canopy transpiration parameterization for 142 2.8 11 vineyards in the California Central Valley. Irrigation Science, 2022, 40, 575-591. Application of a remote-sensing three-source energy balance model to improve evapotranspiration partitioning in vineyards. Irrigation Science, 2022, 40, 593-608. 2.8 Towards Routine Mapping of Crop Emergence within the Season Using the Harmonized Landsat and 144 4.0 11 Sentinel-2 Dataset. Remote Sensing, 2021, 13, 5074.

#	Article	IF	CITATIONS
145	Modeling the Effects of the Urban Built-Up Environment on Plant Phenology Using Fused Satellite Data. Remote Sensing, 2017, 9, 99.	4.0	10
146	Improving the spatiotemporal resolution of remotely sensed ET information for water management through Landsat, Sentinel-2, ECOSTRESS and VIIRS data fusion. Irrigation Science, 2022, 40, 609-634.	2.8	10
147	Estimation of the parameter error propagation in inversion based BRDF observations at single sun position. Science in China Series D: Earth Sciences, 2000, 43, 9-16.	0.9	9
148	Unmanned airborne thermal and mutilspectral imagery for estimating evapotranspiration in irrigated vineyards. , 2017, , .		9
149	Evaluating a spatiotemporal shape-matching model for the generation of synthetic high spatiotemporal resolution time series of multiple satellite data. International Journal of Applied Earth Observation and Geoinformation, 2021, 104, 102545.	2.8	8
150	Predicting spatialâ€ŧemporal patterns of diet quality and large herbivore performance using satellite time series. Ecological Applications, 2022, 32, e2503.	3.8	8
151	An illumination correction algorithm on Landsat-TM data. , 2010, , .		7
152	The Retrieval of 30-m Resolution LAI from Landsat Data by Combining MODIS Products. Remote Sensing, 2018, 10, 1187.	4.0	7
153	Estimation of surface thermal emissivity in a vineyard for UAV microbolometer thermal cameras using NASA HyTES hyperspectral thermal, and landsat and AggieAir optical data. , 2019, 11008, .		7
154	Time-series clustering of remote sensing retrievals for defining management zones in a vineyard. Irrigation Science, 2022, 40, 801-815.	2.8	6
155	Constraints and Opportunities for Detecting Land Surface Phenology in Drylands. Journal of Remote Sensing, 2021, 2021, .	6.7	6
156	Application of the vineyard data assimilation (VIDA) system to vineyard root-zone soil moisture monitoring in the California Central Valley. Irrigation Science, 0, , 1.	2.8	6
157	Parameter error propagation in BRDF derived by fitting multiple angular observations at single sun position. , 0, , .		5
158	Monitoring water and carbon fluxes at fine spatial scales using HysplRI-like measurements. , 2012, , .		5
159	Integrating remote sensing data from multiple optical sensors for ecological and crop condition monitoring. , 2013, , .		5
160	Inter-annual variability of land surface fluxes across vineyards: the role of climate, phenology, and irrigation management. Irrigation Science, 2022, 40, 463-480.	2.8	5
161	Remote Sensing of Vegetation with Landsat Imagery. Taylor & Francis Series in Remote Sensing Applications, 2011, , 3-29.	0.0	4
162	Improving phenological monitoring of winter wheat by considering sensor spectral response in spatiotemporal image fusion. Physics and Chemistry of the Earth, 2020, 116, 102859.	2.9	4

#	Article	IF	CITATIONS
163	Multiscale Assessment of Agricultural Consumptive Water Use in California's Central Valley. Water Resources Research, 2021, 57, e2020WR028876.	4.2	4
164	Influence ofÂmodelingÂdomain and meteorological forcingÂdataÂonÂdaily evapotranspiration estimates from aÂShuttleworth–Wallace modelÂusingASentinel-2 surface reflectance data. Irrigation Science, 0, , 1.	2.8	4
165	Evaluating different metrics from the thermal-based two-source energy balance model for monitoring grapevine water stress. Irrigation Science, 0, , .	2.8	4
166	Spatial and temporal information fusion for crop condition monitoring. , 2016, , .		3
167	Mapping evapotranspiration at multiple scales using multi-sensor data fusion. , 2016, , .		3
168	Mapping Wildland Fire Scar Using Fused Landsat and MODIS Surface Reflectance. , 2006, , .		2
169	An Angular Index to Indicate Surface Heterogeneous Behaviors from MODIS. , 2008, , .		2
170	Influence of angular effects and adjustment on medium resolution sensors for crop monitoring. , 2013, , .		2
171	Downscaling of coarse resolution LAI products to achieve both high spatial and temporal resolution for regions of interest. , 2015, , .		2
172	Daily mapping of Landsat-like LAI and correlation to grape yield. , 2016, , .		2
173	Continuous evapotranspiration monitoring and water stress at watershed scale in a Mediterranean oak savanna. Proceedings of SPIE, 2016, , .	0.8	2
174	Evaluating Yield Variability of Corn and Soybean Using Landsat-8, Sentinel-2 and Modis in Google Earth Engine. , 2019, , .		2
175	Remote Sensing for Agriculture. Springer Remote Sensing/photogrammetry, 2021, , 7-24.	0.4	2
176	Estimating Evapotranspiration of Mediterranean Oak Savanna at Multiple Temporal and Spatial Resolutions. Implications for Water Resources Management. Remote Sensing, 2021, 13, 3701.	4.0	2
177	Integrating Landsat with MODIS Products for Vegetation Monitoring. , 2013, , 247-261.		2
178	Improvement on the inversion of kernel-driven BRDF model. Science Bulletin, 1999, 44, 76-79.	1.7	1
179	Normalizing Landsat and ASTER data using MODIS data products for forest change detection. , 2010, , .		1
180	Evaluating the temporal stability of synthetically generated time-series for crop types in Central Germany. , 2015, , .		1

11

#	Article	IF	CITATIONS
181	A thermal-based remote sensing modelling system for estimating crop water use and stress from field to regional scales. Acta Horticulturae, 2016, , 71-80.	0.2	1
182	Assessment of Predictive Ability of Starfm Based on Different Modis-Landsat Image Pair Date. , 2018, , .		1
183	The Moderate Resolution Imaging Spectroradiometer (MODIS) BRDF and albedo product: preliminary results. , 0, , .		1
184	Improving access to MODIS biophysical science products for NACP investigators. , 2007, , .		0
185	Monitoring vegetation phenology using improved MODIS products. , 2007, , .		0
186	An integrated approach for high spatial resolution mapping of water and carbon fluxes using multi-sensor satellite data. Proceedings of SPIE, 2012, , .	0.8	0
187	Coupling of phenological information and synthetically generated time-series for crop types as indicator for vegetation coverage information. , 2015, , .		0
188	Longterm daily fieldscale evapotranspiration estimation using multisatellite data fusion in an intensively drained agricultural area in South Dakota, USA. , 2016, , .		0
189	Study of water use in agricultural landscapes at high spatiotemporal resulotion. , 2016, , .		0
190	Using Daily Stand-Scale Evapotranspiration (ET) Estimated From Remotely Sensed Data to Investigate Drought Impact on ET in a Temporate Forest in the Central Us. , 2019, , .		0